# Depth of α-Synuclein in a Bilayer Determined by Fluorescence, Neutron Reflectometry, and Computation

Candace M. Pfefferkorn,[†] Frank Heinrich,[¶‖] Alexander J. Sodt,[‡] Alexander S. Maltsev,[§] Richard W. Pastor,[‡] and Jennifer C. Lee[†*]

[†]Laboratory of Molecular Biophysics, [‡]Laboratory of Computational Biology, National Heart, Lung, and Blood Institute, and [§]Laboratory of Chemical Physics, National Institute of Diabetes and Digestive and Kidney Diseases, National Institutes of Health, Bethesda, Maryland; [¶]Department of Physics, Carnegie Mellon University, Pittsburgh, Pennsylvania; and [‖]Center for Neutron Research, National Institute of Standards and Technology, Gaithersburg, Maryland

ABSTRACT α-Synuclein (α-syn) membrane interactions are implicated in the pathogenesis of Parkinson's disease. Fluorescence and neutron reflectometry (NR) measurements reveal that α-syn penetrates ~9–14 Å into the outer leaflet of the bilayer, with a substantial portion of the membrane-bound polypeptide extending into the aqueous solvent. For the first time, to our knowledge, we used NR to obtain direct quantitative evidence of α-syn-induced membrane thinning. To examine the effect of specific residues on membrane penetration depths, we used a series of W4-containing N-terminal peptides. We identified that the first 15 residues (P15) nearly recapitulate the features of the full-length protein (*i.e.,* partition constants, molecular mobility, and insertion of the W4 side chain into the bilayer), and found that as few as the first four N-terminal residues are sufficient for vesicle binding. Although at least one imperfect amphipathic repeat sequence (KAKEGV) is required for α-helical formation, secondary structural formation has little effect on membrane affinity. To develop an N-terminal α-syn model for bilayer interactions, we performed molecular-dynamics simulations of the P15 peptide submerged in a bilayer. The simulation results are highly consistent with experimental data indicating a broad low-energy region (8.5–14.5 Å) for W4 insertion.

## INTRODUCTION

Parkinson's disease (PD) is a prevalent age-related neurodegenerative disease typified by the presence of intracellular brain deposits called Lewy bodies (LBs) (1). Although the molecular mechanisms of PD are ill-defined, several lines of evidence link its pathogenesis to the protein α-synuclein (α-syn) (1). Of note, α-syn is the primary proteinaceous component of LBs (1), and missense mutations in α-syn (A30P, E46K, and A53T) as well as gene duplications and triplications result in early-onset PD (2). Although α-syn has been characterized as unstructured (3) or partially helical (4) in solution, it is the β-sheet, aggregated (fibrillar) form that is found in LBs (5,6). An understanding of how α-syn converts from a benign, soluble conformation to its disease-related fibrillar state requires detailed biochemical and biophysical studies of α-syn aggregation and the effects of solution conditions on its behavior.

The role of membranes is particularly relevant because they are ubiquitous in vivo, alter the protein-folding landscape, and can promote protein-protein interactions by serving as a two-dimensional folding template (7). Indeed, membranes have been shown to modulate both α-syn structure (disordered → α-helical) and aggregation kinetics in vitro (8–11). The relationship between membranes and α-syn amyloid formation is further bolstered by both genetic evidence that early-onset mutations have differential membrane-binding properties (12) and the observation that prefibrillar α-syn can permeabilize membranes (13–15).

The primary structure of α-syn has distinct characteristics that provide insight into its propensity to adopt various conformations under different solution conditions. The N-terminal 89 residues contain seven imperfect amphipathic repeats (KXKEGV; Fig. 1) that are reminiscent of sequences found in membrane-associated α-helical exchangeable apolipoproteins (16,17). Indeed, an α-helical propensity of the N-terminal region (residues 6–37) has been predicted by NMR chemical shift mapping data (18). The central region (residues 61–95), otherwise called the nonamyloid β component, is composed of nonpolar side chains and is important for protein aggregation (19). In contrast, the C-terminal domain is highly acidic and does not generally associate with membranes (20,21) or form part of the fibril core (22–25).

Although it has been shown that α-syn adopts an extended α-helical conformation upon membrane binding (26), several recent works point to the importance of the N-terminal domain. NMR studies of SUV-bound α-syn show that N-terminal conformation is dependent on α-syn/lipid stoichiometry (27). Circular dichroism (CD) and isothermal titration calorimetry experiments further revealed that the first 25 residues are likely involved in membrane-induced polypeptide folding (28). The biological relevance of an N-terminally membrane-associated α-syn is underscored by a recent study that used *Saccharomyces cerevisiae* as a cellular model in which α-syn-induced cell toxicity is mediated by the presence of N-terminal

*Submitted October 14, 2011, and accepted for publication December 30, 2011.*

*Correspondence: leej4@mail.nih.gov

Editor: Heinrich Roder.



0006-3495/12/02/0613/9 $2.00

doi: 10.1016/j.bpj.2011.12.051


FIGURE 1 Schematic representation of full-length α-syn, with the seven amphipathic amino acid imperfect repeat regions (KXKEGV) colored in gray. The sequence for N-terminal peptides is also given with the single tryptophan site (W4; *bold*), lysine residues (*italics*), and imperfect repeat region (*underlined*) highlighted.

residues (29). A scenario in which α-syn associates with the membrane at the far N-terminus is attractive because exposed central and C-terminal domains would thus be available for binding to other biomolecules. For example, α-syn is proposed to promote soluble *N*-ethylmaleimide-sensitive factor attachment protein receptor (SNARE) complex assembly via N-terminal membrane association and C-terminal interaction with the SNARE protein, synaptobrevin (30). A C-terminal interaction site for membrane-bound α-syn with glucocerebrosidase, a lysosomal hydrolase, has also been proposed (31).

Despite the substantial attention paid to α-syn membrane-binding properties (26), direct measurements of the penetration depth of α-syn within the bilayer and the role of specific N-terminal residues in mediating membrane association have not yet been reported. Moreover, although numerous studies have focused on polypeptide conformational dynamics upon α-syn-membrane binding (18,32–42), insights into how the protein interaction influences phospholipid bilayer structure remain limited. Such information would not only aid the development of an atomic-level picture of the α-syn-membrane interface, it would also help elucidate the role of N-terminal residues and changing bilayer properties in α-syn function and dysfunction.

In this work, we determined the N-terminal α-syn bilayer penetration depth of residue 4 (W4) by measuring the fluorescence changes of a single Trp mutant (F4W) upon binding to phospholipid vesicles containing the heavy-atom, collisional quencher bromine. W4 is an excellent probe of protein-bilayer interactions because not only is the indole side chain exquisitely responsive to local environment and conformation (43–46), it has also been established as a high-affinity membrane-binding site in the full-length protein, and, of more importance, this side-chain substitution does not alter equilibrium protein-membrane binding properties (20).

To further assess the depth of α-syn in a bilayer from the perspective of the membrane, we employed neutron reflectometry (NR) and a surface-stabilized sparsely tethered bilayer lipid membrane (stBLM) (47,48). The bombardment of neutrons on a material can provide pertinent structural information. Neutrons are particularly well suited for the study of biological materials because, unlike electrons and x-rays, neutrons have highly disparate scattering length densities (nSLD) for hydrogen and its isotope deuterium with de Broglie wavelengths on a molecular length scale (~5 Å) (49). Organic layers that contain different numbers of hydrogen atoms, such as lipid headgroups and hydrocarbons in a membrane, can be readily distinguished and characterized. One advantage unique to NR is that both membrane-bound α-syn and changes in phospholipid bilayer properties resulting from protein binding can be monitored simultaneously. In this work, we used NR to measure the depth of α-syn in an stBLM, as well as membrane-protein volume occupancies and changes in membrane thickness resulting from protein binding.

To investigate the involvement of specific N-terminal residues in membrane penetration, we monitored the local environment of N-terminal α-syn polypeptides containing W4 (residues 1–4 (P4), 1–6 (P6), 1–10 (P10), and 1–15 (P15); Fig. 1). In particular, we examined how membrane binding is modulated by the presence of the consensus amphipathic repeat (residues 10–15) and positive charges (K6 and K10). In addition, we used CD and $^1$H NMR spectroscopies to assess the role of other (nonfluorescent) residues in secondary structural formation and membrane interactions, respectively. Finally, we performed all-atom simulations of P15 in a bilayer to provide a molecular framework of N-terminal residue interactions with the phospholipid bilayer.

## MATERIALS AND METHODS

Details about the materials and methods used in this work are provided in the Supporting Material.

## RESULTS AND DISCUSSION

### α-Syn bilayer penetration probed by W4

It is well established that the penetration of Trp residues into a lipid bilayer can be monitored via fluorescence quenching by molecules (such as bromine) that are incorporated at specific sites in the lipid hydrocarbon chain (50–53). To determine the penetration depth of the N-terminus of α-syn in the bilayer, we measured W4 fluorescence in the presence of vesicles containing brominated lipids. The bromine positions in the hydrocarbon acyl-chain are illustrated in Fig. 2 *a*. The $Br_{6\text{-}7}$PC, $Br_{9\text{-}10}$PC, and $Br_{11\text{-}12}$PC, W4 quenching data can be correlated to approximate Trp locations at 11, 8.3, and 6 Å above the bilayer center, respectively (54).

Fig. 2 *b* shows representative emission spectra for F4W in the presence of 1:1 POPA/POPC vesicles (*black*) and 1:1 POPA/POPC vesicles containing 30% $Br_{9\text{-}10}$PC (*gray*). Substantial quenching (~46%) is observed as W4 partitions into the bilayer. A comparison of the steady-state W4 fluorescence quenching from vesicles containing brominated

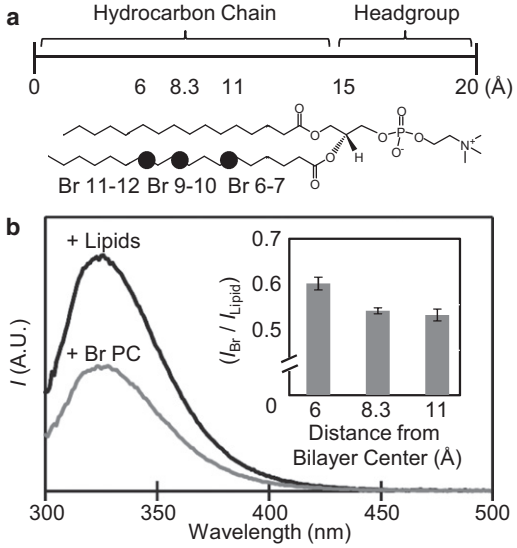


FIGURE 2 Tryptophan side-chain penetration into the vesicle bilayer. (*a*) Structure of PC phospholipid with positions of bromines highlighted. (*b*) Steady-state fluorescence of F4W α-syn (5 μM in 10 mM NaPi, 100 mM NaCl buffer, pH 7.4, 25°C) in the presence of 1:1 POPA/POPC vesicles (*black*) and 1:1 POPA/POPC vesicles containing 30% bromine-labeled $Br_{9\text{-}10}$PC lipids (*gray*; lipid/protein molar ratio = 300). The inset shows the relative quenching of F4W steady-state fluorescence in the presence of 1:1 POPA/POPC vesicles containing 30% $Br_{6\text{-}7}$PC, $Br_{9\text{-}10}$PC, and $Br_{11\text{-}12}$PC. Relative quenching is reported as $I_{Br}/I_{Lipid}$, where $I_{Br}$ and $I_{Lipid}$ are the integrated steady-state emissions (325–400 nm) in the presence of vesicles with and without brominated lipids, respectively. Error bars represent the SD of the mean for $n \geq 3$ independent measurements.

lipids ($I_{Br}$) with unlabeled POPA/POPC vesicles ($I_{Lipid}$) for each of the bromine labeling positions is provided in the inset of Fig. 2 *b* ($I_{Br}/I_{Lipid}$ = 0.53 ± 0.05, 0.54 ± 0.01, 0.60 ± 0.01, for $Br_{6\text{-}7}$PC, $Br_{9\text{-}10}$PC, and $Br_{11\text{-}12}$PC, respectively). We also obtained comparable values for relative F4W bromine quenching using time-resolved fluorescence measurements (data not shown). In contrast to the site-specific quenching of the integral membrane protein OmpA (51), substantial Trp quenching was measured for all sites, with a modest preference for positions closer to the headgroups. This large range (6–11 Å) of α-syn penetration distances may reflect heterogeneity within the bilayer. It is also plausible that the lipids themselves are dynamic, translating to and from the bilayer center.

## NR as a dual probe of α-synuclein and membrane structure

To obtain definitive information on α-syn membrane penetration depth, we performed NR experiments employing an stBLM. Because NR can simultaneously probe the protein and the bilayer, we were able to establish values for protein extension into the bulk solvent, protein-membrane occupancy, and changes in membrane thickness. We measured the neutron reflection of an stBLM (47,48,55) composed of a 1:1 molar ratio of POPA/POPC in the presence and absence of α-syn. This lipid composition was chosen to facilitate comparison with our previous (20) and current studies on vesicles, and because α-syn has been demonstrated to have a high affinity for POPA (8,56). We collected a minimum of two reflectivity curves for each condition using either $H_2O$- or $D_2O$-based buffer.

Fig. 3 *a* shows the neutron reflection data for the stBLM alone and in the presence of α-syn in $H_2O$ (*red*) and $D_2O$ (*blue*) buffers. For both solvents, the residuals between reflectivity curves with and without protein exceed 5 standard deviations (SDs) at low momentum transfer values and average 1–3 SDs up to a momentum transfer $q_z = 0.15$ Å$^{-1}$. These significant changes in the measured reflectivity upon the addition of protein manifest in a modulation of the amplitude and frequency of the Kiessig fringes. Fits based on a continuous distribution model (57) (see Supporting Material) are shown as solid lines. Along with a schematic view of the stBLM, Fig. 3 *b* shows a cross-sectional profile

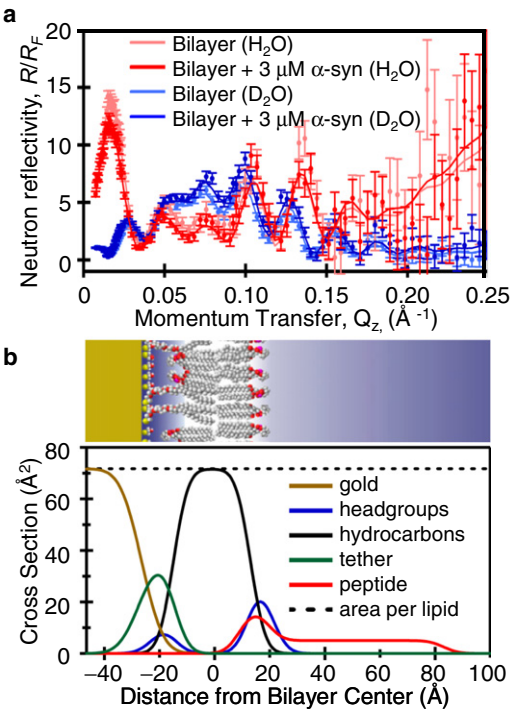


FIGURE 3 Neutron reflection of a sparsely tethered POPA/POPC bilayer lipid membrane (stBLM) and changes resulting from the addition of α-syn. (*a*) Neutron reflectivity ($R/R_F$) for a POPA/POPC stBLM in the absence and presence of α-syn (3 μM in 10 mM NaPi, 100 mM NaCl, pH 7.4) in $H_2O$ and $D_2O$. Continuous distribution model fits to the data are shown as solid lines. Error bars represent the 68% confidence intervals for the measured reflectivity based on Poisson statistics. (*b*) Top: Schematic of stBLM with additional solid substrate portions (Si, SiOx, Cr, and Au) partially omitted. Bottom: Simplified molecular distributions for each organic interface layer of the POPA/POPC stBLM and α-syn obtained from the best fit of reflectivity data to the continuous distribution model. The dotted line denotes a reference value for area per lipid. Data for the Si substrate and the SiOx, Cr, and Au layer are partially omitted.

of the organic interfaces extracted from the best fits to the data (see Table S1 for fit parameters and associated 68.2% confidence intervals). For simplicity, a number of submolecular groups that were modeled separately have been combined in this representation.

Before incubation with protein, the substrate and neat bilayer parameters fall within expected values with an inner and outer bilayer leaflet thickness of 14.4 and 14.8 Å, respectively. Upon protein addition, the reflectivity data indicate that substantial α-syn (15% volume occupancy) is associating with the membrane at both the headgroup region and the hydrocarbon region (a 13.1 Å thick protein region penetrating 4.2 Å into the outer-leaflet hydrocarbons), consistent with bromine quenching data. α-Syn (6.8% volume occupancy) was also found to extend well into the aqueous region (63.1 Å). Notably, the association of α-syn resulted in a sizable reduction (1.44 Å) in membrane bilayer thickness.

Although the exact protein conformation(s) cannot be determined, by comparison with the diameter of an α-helix (12 Å), the finding of a ~13 Å protein layer in the outer leaflet of the stBLM is consistent with an α-helical structure. This penetration depth is also in agreement with results from electron paramagnetic resonance accessibility experiments (40) suggesting that the center of the α-helix is located near the phosphate groups. The observation of protein density in the aqueous environment indicates that only a portion of the α-syn polypeptide is anchored to the outer leaflet, leaving other protein regions solvent-accessible. Based on the estimated mean distances of ~33–43 Å between C-terminal residues 94–136 (58), we suggest that the ~63 Å solvent-exposed region is comprised of more residues than are found in the far C-terminal acidic domain. One possibility, in accordance with recent NMR results (27), is that N-terminal residues are membrane-bound while more-central and C-terminal residues remain free in solution.

The observation that bilayer thickness is reduced upon α-syn association is intriguing because protein-induced membrane perturbations have been linked to PD (59–62). Although the absolute value of 1.44 Å appears to be modest, we note that this value represents an average over the whole stBLM surface area, and localized thinning could be much higher. If only areas proximal to the bound protein were affected, thinning would be quite substantial. α-Syn penetration into the outer leaflet may explain why the protein has a preference for highly curved membranes (8) and can even induce membrane curvature under certain conditions (63). Specifically, the shallow insertion could induce membrane curvature to compensate for changes to headgroup packing and for differences in the area between the inner and outer leaflets (64,65). Additional work will be required to elucidate the molecular mechanism by which thinning occurs, but it is clear that a lipid reorganization occurs (66), and it is even possible, as recently proposed by Reynolds et al. (67), that the protein extracts lipids from the bilayer.

## Membrane affinities and Gibbs free energies

To evaluate the role of specific N-terminal residues in membrane binding, we compared the membrane-binding affinities of a series of α-syn peptides composed of the first 15 residues (P4, P6, P10, and P15) with that of the full-length protein using Trp fluorescence (Fig. 4). We sought to determine whether these isolated segments could serve as membrane anchors (vide supra). Although the introduction of W4 has been shown to have little effect on full-length α-syn membrane-binding properties (20), we first ascertained that W4 also had minimal perturbations in P15 (Fig. S1).

Before the addition of vesicles, the fluorescence spectra for all peptides and the full-length protein are similar, with mean wavelengths ($<\lambda>$) consistent with a water-exposed Trp side chain ($<\lambda>$ = 360–363 nm; for model compound, *N*-acetyl-tryptophanamide (NATA), $<\lambda>$ = 365 nm). However, in the presence of vesicles, spectral changes are observed as a function of peptide length (P15 > P10 > P6), reflecting different environments for the W4 side chain (Fig. 4). For P6, P10, and P15, increases in integrated intensity ($I$) and spectral blue shifts suggest increased side-chain rigidity as W4 interacts with the hydrophobic membrane interior (Table S2). In contrast, even in the presence of high vesicle concentrations (2.5 mM), no significant change in $<\lambda>$ or $I$ was observed in the P4 peptide, indicating minimal deviations in the W4 microenvironment. Changes in $I$ (~2.0-fold increase) and $<\lambda>$ (17 nm blue shift) for P15 are highly reminiscent of the full-length protein (~2.0-fold increase, 22 nm blue shift) highlighting that the association of the first 15 residues results in similar W4 microenvironments.

Using $<\lambda>$ data, we extracted apparent membrane partition constants ($K_p^{app}$) and Gibbs free energies ($\Delta G$) using a membrane partition equilibrium model (68) (Table S2).

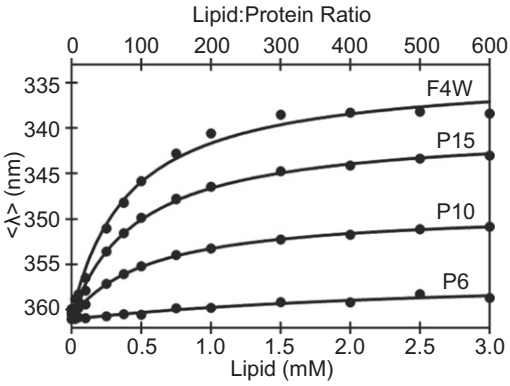


FIGURE 4 Comparison of vesicle binding of single Trp containing full-length α-syn (F4W) and N-terminal peptides. Mean wavelength ($<\lambda>$) as a function of the lipid/protein ratio (*top axis*) and lipid concentration (*bottom axis*) for F4W and α-syn peptides (5 μM α-syn polypeptides, 0–3 mM 1:1 POPA/POPC in 10 mM NaPi, 100 mM NaCl buffer, pH 7.4, 25°C). Fits to the membrane partition equilibrium model are shown as solid lines.

Despite differences in absolute $<\lambda>$, reflecting variations in W4 microenvironments, the $K_p^{app}$ and $\Delta G$ values for both P10 and P15 were quite similar to that observed for full-length $\alpha$-syn ($K_p^{app}$= 4100, 3600, and 2900 $M^{-1}$; $\Delta G$ = −7.3, −7.2, and −7.1 kcal/mol for full-length $\alpha$-syn, P15, and P10, respectively). However, in the case of P6, we observe substantial decreases in $K_p^{app}$ and $\Delta G$ (600 $M^{-1}$ and −6.3 kcal/mol, respectively). The measured free energies for all variants are comparable to those of membrane-associating peptides (~−2.3 to −8.9 kcal/mol) (68). Although the $\Delta G$ difference for P6 and P10 (−0.8 kcal/mol) is consistent with the addition of one lysine in P10 (which contributes ~−1 kcal/mol due to favorable electrostatic side-chain-headgroup interactions) (69), the difference between P10 and P15 is very small (−0.1 kcal/mol) even though P15 also contains one extra lysine.

## Role of the amphipathic repeat in helical formation

We collected CD spectra for P10 and P15 to examine secondary structure formation from random coil to $\alpha$-helix. At saturating vesicle concentrations, P10 exhibited a <15% $\alpha$-helical content, compared with ~56% in P15 (Fig. 5). The propensity for the isolated P15 polypeptide to associate and adopt $\alpha$-helical secondary structure upon membrane interaction can be rationalized by the preference of lysine residues (K6, K10, and K12) to flank the anionic PA headgroups creating an interface between water-exposed, charged residues (D2 and E13) and lipid-facing, nonpolar residues (V3, W4, G7, L8, A11, and V14). Indeed, N-terminal $\alpha$-syn residues 6–15 are predicted by NMR chemical shift mapping to have a substantial preference for $\alpha$-helical formation (18). Although the amphipathic repeat in P15 is only six residues (KAKEGV), the observed $\alpha$-helical content would correspond to at least eight, suggesting that the presence of the repeat promotes $\alpha$-helical structure into other N-terminal residues.

We suggest that the enhancement in $\Delta G$ resulting from the addition of K12 in P15 is counterbalanced by some losses in entropy resulting from helical structural formation. Many studies have shown that all seven amphipathic repeats in $\alpha$-syn are involved in membrane binding (26). Because both P15 and the full-length protein have similar $\Delta G$ values, we propose that any independent repeat is sufficient for bilayer association. This proposal is supported by work demonstrating that other, isolated $\alpha$-syn polypeptides can indeed bind to membranes (28,70). Regardless of the exact contributions to free-energy changes, the CD results demonstrate the importance of the full amphipathic repeat sequence in $\alpha$-helical formation. Using CD data, we determined $K_p^{app}$ values for P15 and the full-length protein ($K_p^{app}$ = 1600 $M^{-1}$ and 2000 $M^{-1}$, respectively). These $K_p^{app}$ values are a factor of 2 smaller than those extracted from fluorescence data, indicating that W4 partitions into the bilayer at lipid concentrations lower than those required for protein secondary structure development.

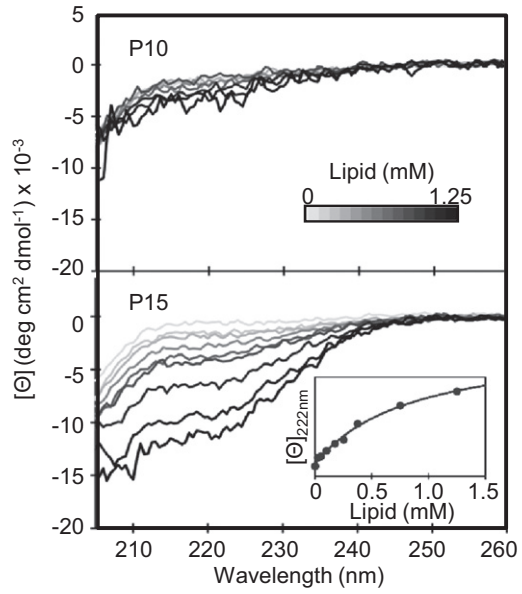


FIGURE 5 Vesicle-induced secondary structural formation of P10 and P15 peptides. CD spectra for P10 (*top*) and P15 (*bottom*) as a function vesicle addition (10 $\mu$M peptide, 10 mM NaPi, 100 mM NaCl buffer, pH 7.4, 25°C, 0–1.25 mM 1:1 POPA/POPC). Inset: P15 membrane-binding curve generated from the mean residue ellipticity ([Θ]) at 222 nm. A fit to the membrane partition equilibrium model is shown as a solid line.

## Tryptophan microenvironment at the bilayer interface

Insights into Trp side-chain mobility as a function of polypeptide length were gained through time-resolved anisotropy experiments. In the absence of vesicles, all $\alpha$-syn peptides and F4W exhibit small initial anisotropies ($r_o$ = 0.03–0.06) with nanosecond rotational correlation times ($\tau_C$ = 0.5–0.9 ns) and zero residual anisotropy ($r_\infty$; Fig. 6 a). These values are consistent with a solvent-exposed and freely rotating Trp side chain. Upon vesicle addition, all peptides and F4W show significant increases in $r_o$, $r_\infty$, and $\tau_C$, indicative of peptide-vesicle interaction and restriction in rotational freedom of W4 upon membrane association. In the presence of vesicles, $r_o$ was greatest for F4W, followed by P15, P10, P6, and P4 (0.16, 0.14, 0.14, 0.11, and 0.09, respectively). Minimal decay from $r_o$ was observed on the timescale of F4W fluorescence lifetime in the presence of vesicles ($<\tau>$ = 3.6 ns (20)).

Unexpectedly, our anisotropy data reveal that P4 is also interacting with the vesicles. Increases in $r_o$ and $r_\infty$ upon vesicle addition indicate that P4 is part of a larger, vesicle-bound complex that has a slower tumbling time than P4 alone in solution. It is possible that we did not observe a steady-state spectral shift because, although P4 is bound, W4 does not embed into the hydrophobic

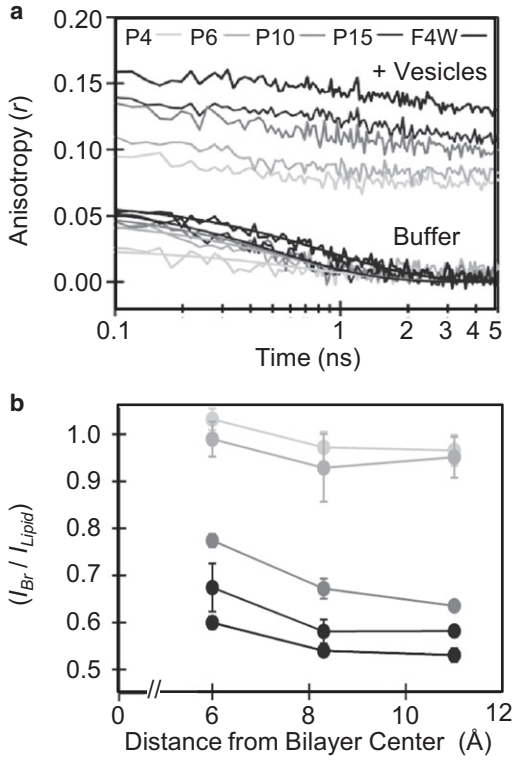


FIGURE 6 W4 time-resolved anisotropy and bilayer penetration of F4W and N-terminal peptides. (*a*) Time-resolved anisotropy decays for F4W and $\alpha$-syn peptides 1–15 (P15), 1–10 (P10), 1–6 (P6), and 1–4 (P4) (dark to light, respectively) in the absence and presence of phospholipid vesicles (5 $\mu$M $\alpha$-syn polypeptides, 0 and 1.5 mM 1:1 POPA/POPC in 10 mM NaPi, 100 mM NaCl buffer, pH 7.4, 25°C). The data represent the average of $n \geq 3$ measurements. Single exponential fits to anisotropy decays measured in solution are shown as solid lines. (*b*) Relative quenching of W4 steady-state fluorescence for F4W and N-terminal peptides in the presence of 1:1 POPA/POPC vesicles containing 30% $Br_{6\text{-}7}$PC, $Br_{9\text{-}10}$PC, and $Br_{11\text{-}12}$PC (lipid/protein ratio = 300). Relative quenching is reported as $I_{Br}/I_{Lipid}$, where $I_{Br}$ and $I_{Lipid}$ are the integrated steady-state emissions (325–400 nm) in the presence of vesicles with and without brominated lipids, respectively. Error bars represent the SD of the mean for $n \geq 3$ independent measurements.

environment of hydrocarbon chain. Furthermore, the expected increase in intensity upon restriction of the indole rotational motion could be offset by the proximity of the fluorophore to the negatively charged headgroups, which would lead to a quantum yield decrease (71). To corroborate this result, we turned to $^1$H NMR spectroscopy. By examining changes in $^1$H chemical shifts upon vesicle addition, we indeed found that P4 interacts with the membrane and that the binding affinity is dependent on the polypeptide length (P15 > P10 > P6 > P4; Fig. S2).

## N-terminal $\alpha$-synuclein peptide bilayer penetration

To determine the effect of N-terminal residues on the bilayer penetration depth, we measured the steady-state fluorescence of P15, P10, P6, and P4 in the absence and presence of vesicles containing $Br_{6\text{-}7}$PC, $Br_{9\text{-}10}$PC, and $Br_{11\text{-}12}$PC. Fig. 6 *b* provides a comparison of W4 fluorescence intensities for all $\alpha$-syn polypeptides in the presence of unlabeled ($I_{Lipid}$) and bromine-containing ($I_{Br}$) POPA/POPC vesicles. Consistent with steady-state Trp measurements, P4 emission is not significantly quenched in the presence of brominated lipids. Because anisotropy and NMR measurements indicate that P4 is membrane-associated, these data suggest that W4 is interacting with the headgroups. Decreases in P6 fluorescence are modest but measurable, indicating that at least a small fraction of P6 embeds into the hydrocarbon chain region. In contrast, the quenching values for P10 and P15 approach those of the full-length protein. Substantial decreases in Trp intensity are observed for all bromine positions, demonstrating that a considerable proportion of W4 side chains resides ~6–11 Å above the bilayer center. Although we observed quenching at all bromine positions, there were modest increases as a function of distance from the center of the bilayer, indicating a slight preference for conformations in which W4 is closer to the headgroup region.

## All-atom simulations at the P15-bilayer interface

Taken together, our data demonstrate that the $\alpha$-helical forming P15 could serve as a minimal model for N-terminal $\alpha$-syn-membrane interactions. Accordingly, we performed molecular-dynamics simulations of the P15 peptide submerged in a bilayer for atomic-level insights. The lowest-energy structures reveal that residues M1, W4, and L8 are the deepest within the bilayer, and residues D2, K6, S9, K10, and E13 are primarily solvent-exposed. Of interest, L8 and S9 exhibit the smallest deviations in position, suggesting that these residues may serve as a pivot point for P15, which has a slight N-terminal tilt into the bilayer. Likewise, greater deviations in the position of far N-terminal residues (M1–M5) suggest that this region is dynamic and reversibly permeates the bilayer surface.

Fig. 7 shows the free energy for bilayer penetration of the P15 peptide for both the peptide center of geometry (COG) and the W4 COG. The simulations indicate a broad region corresponding to high relative probability for the W4 COG (~5.5–11.5 Å above the bilayer center). These results are in extremely good agreement with W4 quenching experiments (~6–11 Å above the bilayer center). Although the simulated P15 membrane-bound conformations exhibit greater $\alpha$-helical content than that measured by CD, complicating a direct comparison with the experiments, it is plausible that a peptide conformational heterogeneity exists in which both fully and partially $\alpha$-helical P15 populations are in equilibrium. Nevertheless, both experimental and computational results show that this membrane-bound N-terminal peptide samples multiple regions of the bilayer. The presence of P15 in the bilayer does induce membrane

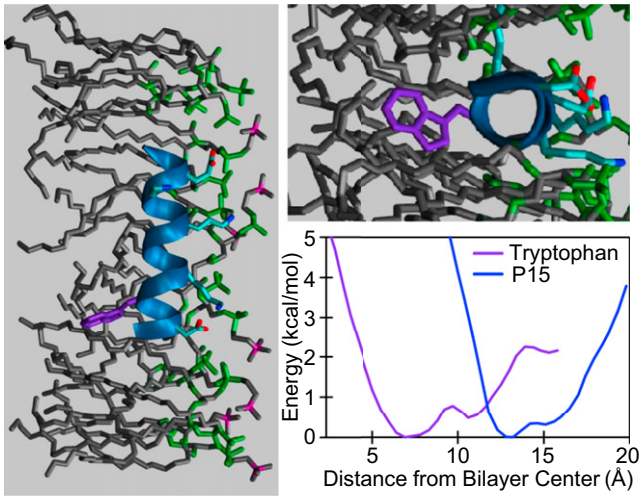


FIGURE 7 All-atom simulation of the N-terminal 1–15 $\alpha$-syn peptide (P15) at the bilayer interface. Left: Side view of one of the lowest-energy structures for P15 submerged in a POPA/POPC bilayer. The atomic color scheme for the simulated model is as follows: nitrogen (*dark blue*), oxygen (*red*), lipid carbon (*gray*), lipid oxygen and phosphate (*green*), lipid choline (*light purple*), protein carbon (*light blue*), tryptophan side chain (*purple*), and helix backbone (*blue*). Top right: A close-up view of W4 submerged in the bilayer. Bottom right: Free energy as a function of distance of the W4 side chain (*purple*) and polypeptide (*blue*) center of gravity from the bilayer center.

thinning. The amount of thinning is consistent with what would be expected if the bilayer compresses as the lipid tails fill the void underneath the submerged peptide. Although this result is in agreement with proposed mechanisms (64,65), additional work will be needed to determine how the peptide insertion depth and surface coverage affect membrane thinning.

## CONCLUSION

Using multiple experimental and computational methods, we investigated the depth of bilayer penetration of full-length $\alpha$-syn as well as the participation of specific N-terminal residues. NR measurements obtained with an stLBM show that $\alpha$-syn interacts with the outer-leaflet phospholipid headgroups and hydrocarbons, with additional protein density extending into the aqueous surroundings. Although membrane perturbation is generally found in the presence of oligomeric or protofibrillar $\alpha$-syn, we observed bilayer thinning upon addition of monomeric $\alpha$-syn. Although the completeness of the stBLM was maintained during the course of our experiments (~95–100%), the measured membrane thinning could represent a first step leading to disruption of the bilayer, which has been suggested as a potential pathogenic mechanism.

Our finding that isolated N-terminal peptides can bind to the membrane with an affinity comparable to that of the full-length protein could have biological implications. Natural membranes, such as synaptic vesicles, are decorated with integral and peripheral membrane proteins that limit the amount of free lipid surface (72). Thus, $\alpha$-syn may not be able to bind to the membrane in a fully extended $\alpha$-helical conformation in vivo. Instead, specific regions of $\alpha$-syn may bind to the membrane, leaving other sites available for interaction with other biomolecules (30,31).

## SUPPORTING MATERIAL

Materials and methods, data analysis, two tables, two figures, and references (73–88) are available at http://www.biophysj.org/biophysj/supplemental/S0006-3495(12)00050-1.

We thank G. Piszczek (Biophysics Facility, National Heart, Lung, and Blood Institute (NHLBI)) and D.-Y. Lee (Biochemistry Core Facility, NHLBI) for technical assistance, A. Bax (Laboratory of Chemical Physics, National Institute of Diabetes and Digestive and Kidney Diseases (NIDDK)) for use of the Bruker DMX-600 NMR spectrometer, and D. J. Vanderah (National Institute of Standards and Technology Center (NIST)) for synthesizing the HC18 tether molecule.

This work was supported by the Intramural Research Program of the NHLBI and NIDDK, National Institutes of Health. Research was performed in part at the NIST for Nanoscale Science and Technology.

Certain commercial materials, equipment, and instruments are identified in this work to describe the experimental procedure as completely as possible. In no case does such an identification imply a recommendation or endorsement by NIST, nor does it imply that the materials, equipment, or instruments identified are necessarily the best available for the purpose.

## REFERENCES

1. Lees, A. J., J. Hardy, and T. Revesz. 2009. Parkinson's disease. *Lancet.* 373:2055–2066.
2. Bisaglia, M., S. Mammi, and L. Bubacco. 2009. Structural insights on physiological functions and pathological effects of $\alpha$-synuclein. *FASEB J.* 23:329–340.
3. Weinreb, P. H., W. G. Zhen, …, P. T. Lansbury, Jr. 1996. NACP, a protein implicated in Alzheimer's disease and learning, is natively unfolded. *Biochemistry.* 35:13709–13715.
4. Bartels, T., J. G. Choi, and D. J. Selkoe. 2011. $\alpha$-Synuclein occurs physiologically as a helically folded tetramer that resists aggregation. *Nature.* 477:107–110.
5. Conway, K. A., S. J. Lee, …, P. T. Lansbury, Jr. 2000. Acceleration of oligomerization, not fibrillization, is a shared property of both $\alpha$-synuclein mutations linked to early-onset Parkinson's disease: Implications for pathogenesis and therapy. *Proc. Natl. Acad. Sci. USA.* 97:571–576.
6. Chiti, F., and C. M. Dobson. 2006. Protein misfolding, functional amyloid, and human disease. *Annu. Rev. Biochem.* 75:333–366.
7. Aisenbrey, C., T. Borowik, …, G. Gröbner. 2008. How is protein aggregation in amyloidogenic diseases modulated by biological membranes? *Eur. Biophys. J.* 37:247–255.
8. Davidson, W. S., A. Jonas, …, J. M. George. 1998. Stabilization of $\alpha$-synuclein secondary structure upon binding to synthetic membranes. *J. Biol. Chem.* 273:9443–9449.
9. Zhu, M., and A. L. Fink. 2003. Lipid binding inhibits $\alpha$-synuclein fibril formation. *J. Biol. Chem.* 278:16873–16877.
10. Necula, M., C. N. Chirita, and J. Kuret. 2003. Rapid anionic micelle-mediated $\alpha$-synuclein fibrillization in vitro. *J. Biol. Chem.* 278: 46674–46680.
11. Zhu, M., J. Li, and A. L. Fink. 2003. The association of $\alpha$-synuclein with membranes affects bilayer structure, stability, and fibril formation. *J. Biol. Chem.* 278:40186–40197.

12. Bodner, C. R., A. S. Maltsev, …, A. Bax. 2010. Differential phospholipid binding of α-synuclein variants implicated in Parkinson's disease revealed by solution NMR spectroscopy. *Biochemistry.* 49:862–871.

13. Ding, T. T., S. J. Lee, …, P. T. Lansbury, Jr. 2002. Annular α-synuclein protofibrils are produced when spherical protofibrils are incubated in solution or bound to brain-derived membranes. *Biochemistry.* 41:10209–10217.

14. Volles, M. J., and P. T. Lansbury, Jr. 2002. Vesicle permeabilization by protofibrillar α-synuclein is sensitive to Parkinson's disease-linked mutations and occurs by a pore-like mechanism. *Biochemistry.* 41:4595–4602.

15. Volles, M. J., S. J. Lee, …, P. T. Lansbury, Jr. 2001. Vesicle permeabilization by protofibrillar α-synuclein: Implications for the pathogenesis and treatment of Parkinson's disease. *Biochemistry.* 40:7812–7819.

16. George, J. M., H. Jin, …, D. F. Clayton. 1995. Characterization of a novel protein regulated during the critical period for song learning in the zebra finch. *Neuron.* 15:361–372.

17. Segrest, J. P., M. K. Jones, …, G. M. Anantharamaiah. 1992. The amphipathic helix in the exchangeable apolipoproteins: A review of secondary structure and function. *J. Lipid Res.* 33:141–166.

18. Eliezer, D., E. Kutluay, …, G. Browne. 2001. Conformational properties of α-synuclein in its free and lipid-associated states. *J. Mol. Biol.* 307:1061–1073.

19. El-Agnaf, O. M. A., A. M. Bodles, …, G. B. Irvine. 1998. The N-terminal region of non-A $\beta$ component of Alzheimer's disease amyloid is responsible for its tendency to assume $\beta$-sheet and aggregate to form fibrils. *Eur. J. Biochem.* 258:157–163.

20. Pfefferkorn, C. M., and J. C. Lee. 2010. Tryptophan probes at the α-synuclein and membrane interface. *J. Phys. Chem. B.* 114:4615–4622.

21. Tamamizu-Kato, S., M. G. Kosaraju, …, V. Narayanaswami. 2006. Calcium-triggered membrane interaction of the α-synuclein acidic tail. *Biochemistry.* 45:10947–10956.

22. Chen, M., M. Margittai, …, R. Langen. 2007. Investigation of α-synuclein fibril structure by site-directed spin labeling. *J. Biol. Chem.* 282:24970–24979.

23. Heise, H., W. Hoyer, …, M. Baldus. 2005. Molecular-level secondary structure, polymorphism, and dynamics of full-length α-synuclein fibrils studied by solid-state NMR. *Proc. Natl. Acad. Sci. USA.* 102:15871–15876.

24. Qin, Z., D. Hu, …, A. L. Fink. 2007. Role of different regions of α-synuclein in the assembly of fibrils. *Biochemistry.* 46:13322–13330.

25. Vilar, M., H. T. Chou, …, R. Riek. 2008. The fold of α-synuclein fibrils. *Proc. Natl. Acad. Sci. USA.* 105:8637–8642.

26. Pfefferkorn, C. M., Z. Jiang, and J. C. Lee. 2011. Biophysics of α-synuclein membrane interactions. *Biochim. Biophys. Acta.* 1818:162–171.

27. Bodner, C. R., C. M. Dobson, and A. Bax. 2009. Multiple tight phospholipid-binding modes of α-synuclein revealed by solution NMR spectroscopy. *J. Mol. Biol.* 390:775–790.

28. Bartels, T., L. S. Ahlstrom, …, K. Beyer. 2010. The N-terminus of the intrinsically disordered protein α-synuclein triggers membrane binding and helix folding. *Biophys. J.* 99:2116–2124.

29. Vamvaca, K., M. J. Volles, and P. T. Lansbury, Jr. 2009. The first N-terminal amino acids of α-synuclein are essential for α-helical structure formation in vitro and membrane binding in yeast. *J. Mol. Biol.* 389:413–424.

30. Burré, J., M. Sharma, …, T. C. Südhof. 2010. α-Synuclein promotes SNARE-complex assembly in vivo and in vitro. *Science.* 329:1663–1667.

31. Yap, T. L., J. M. Gruschus, …, J. C. Lee. 2011. α-Synuclein interacts with glucocerebrosidase providing a molecular link between Parkinson and Gaucher diseases. *J. Biol. Chem.* 286:28080–28088.

32. Bisaglia, M., I. Tessari, …, S. Mammi. 2005. A topological model of the interaction between α-synuclein and sodium dodecyl sulfate micelles. *Biochemistry.* 44:329–339.

33. Chandra, S., X. C. Chen, …, T. C. Südhof. 2003. A broken α-helix in folded α-synuclein. *J. Biol. Chem.* 278:15313–15318.

34. Ulmer, T. S., A. Bax, …, R. L. Nussbaum. 2005. Structure and dynamics of micelle-bound human α-synuclein. *J. Biol. Chem.* 280:9595–9603.

35. Drescher, M., G. Veldhuis, …, M. Huber. 2008. Antiparallel arrangement of the helices of vesicle-bound α-synuclein. *J. Am. Chem. Soc.* 130:7796–7797.

36. Borbat, P., T. F. Ramlall, …, D. Eliezer. 2006. Inter-helix distances in lysophospholipid micelle-bound α-synuclein from pulsed ESR measurements. *J. Am. Chem. Soc.* 128:10004–10005.

37. Bussell, Jr., R., and D. Eliezer. 2003. A structural and functional role for 11-mer repeats in α-synuclein and other exchangeable lipid binding proteins. *J. Mol. Biol.* 329:763–778.

38. Georgieva, E. R., T. F. Ramlall, …, D. Eliezer. 2008. Membrane-bound α-synuclein forms an extended helix: Long-distance pulsed ESR measurements using vesicles, bicelles, and rodlike micelles. *J. Am. Chem. Soc.* 130:12856–12857.

39. Jao, C. C., A. Der-Sarkissian, …, R. Langen. 2004. Structure of membrane-bound α-synuclein studied by site-directed spin labeling. *Proc. Natl. Acad. Sci. USA.* 101:8331–8336.

40. Jao, C. C., B. G. Hegde, …, R. Langen. 2008. Structure of membrane-bound α-synuclein from site-directed spin labeling and computational refinement. *Proc. Natl. Acad. Sci. USA.* 105:19666–19671.

41. Ferreon, A. C. M., Y. Gambin, …, A. A. Deniz. 2009. Interplay of α-synuclein binding and conformational switching probed by single-molecule fluorescence. *Proc. Natl. Acad. Sci. USA.* 106:5645–5650.

42. Trexler, A. J., and E. Rhoades. 2009. α-Synuclein binds large unilamellar vesicles as an extended helix. *Biochemistry.* 48:2304–2306.

43. Beechem, J. M., and L. Brand. 1985. Time-resolved fluorescence of proteins. *Annu. Rev. Biochem.* 54:43–71.

44. Chen, Y., and M. D. Barkley. 1998. Toward understanding tryptophan fluorescence in proteins. *Biochemistry.* 37:9976–9982.

45. Ladokhin, A. S., S. Jayasinghe, and S. H. White. 2000. How to measure and analyze tryptophan fluorescence in membranes properly, and why bother? *Anal. Biochem.* 285:235–245.

46. Yu, H. T., M. A. Vela, …, M. D. Barkley. 1995. Microenvironmental effects on the solvent quenching rate in constrained tryptophan derivatives. *J. Am. Chem. Soc.* 117:348–357.

47. Heinrich, F., T. Ng, …, M. Lösche. 2009. A new lipid anchor for sparsely tethered bilayer lipid membranes. *Langmuir.* 25:4219–4229.

48. McGillivray, D. J., G. Valincius, …, M. Lösche. 2007. Molecular-scale structural and functional characterization of sparsely tethered bilayer lipid membranes. *Biointerphases.* 2:21–33.

49. Lakey, J. H. 2009. Neutrons for biologists: a beginner's guide, or why you should consider using neutrons. *J. R. Soc. Interface.* 6 (*Suppl 5*): S567–S573.

50. Bolen, E. J., and P. W. Holloway. 1990. Quenching of tryptophan fluorescence by brominated phospholipid. *Biochemistry.* 29:9638–9643.

51. Kleinschmidt, J. H., and L. K. Tamm. 1999. Time-resolved distance determination by tryptophan fluorescence quenching: Probing intermediates in membrane protein folding. *Biochemistry.* 38:4996–5005.

52. London, E., and G. W. Feigenson. 1981. Fluorescence quenching in model membranes. 1. Characterization of quenching caused by a spin-labeled phospholipid. *Biochemistry.* 20:1932–1938.

53. Markello, T., A. Zlotnick, …, P. W. Holloway. 1985. Determination of the topography of cytochrome $b_5$ in lipid vesicles by fluorescence quenching. *Biochemistry.* 24:2895–2901.

54. McIntosh, T. J., and P. W. Holloway. 1987. Determination of the depth of bromine atoms in bilayers formed from bromolipid probes. *Biochemistry.* 26:1783–1788.

55. Dura, J. A., D. J. Pierce, …, S. H. White. 2006. AND/R: advanced neutron diffractometer/reflectometer for investigation of thin films and multilayers for the life sciences. *Rev. Sci. Instrum.* 77:74301–7430111.

56. Middleton, E. R., and E. Rhoades. 2010. Effects of curvature and composition on $\alpha$-synuclein binding to lipid vesicles. *Biophys. J.* 99:2279–2288.

57. Shekhar, P., H. Nanda, …, F. Heinrich. 2011. Continuous distribution model for the investigation of complex molecular architectures near interfaces with scattering techniques. *J. Appl. Phys.* 110:102216–102216-12.

58. Lee, J. C., R. Langen, …, J. R. Winkler. 2004. $\alpha$-Synuclein structures from fluorescence energy-transfer kinetics: Implications for the role of the protein in Parkinson's disease. *Proc. Natl. Acad. Sci. USA.* 101:16466–16471.

59. Butterfield, S. M., and H. A. Lashuel. 2010. Amyloidogenic protein-membrane interactions: Mechanistic insight from model systems. *Angew. Chem. Int. Ed. Engl.* 49:5628–5654.

60. Kayed, R., Y. Sokolov, …, C. G. Glabe. 2004. Permeabilization of lipid bilayers is a common conformation-dependent activity of soluble amyloid oligomers in protein misfolding diseases. *J. Biol. Chem.* 279:46363–46366.

61. Lashuel, H. A., D. Hartley, …, P. T. Lansbury, Jr. 2002. Neurodegenerative disease: Amyloid pores from pathogenic mutations. *Nature.* 418:291.

62. Quist, A., I. Doudevski, …, R. Lal. 2005. Amyloid ion channels: A common structural link for protein-misfolding disease. *Proc. Natl. Acad. Sci. USA.* 102:10427–10432.

63. Varkey, J., J. M. Isas, …, R. Langen. 2010. Membrane curvature induction and tubulation are common features of synucleins and apolipoproteins. *J. Biol. Chem.* 285:32486–32493.

64. Lagüe, P., B. Roux, and R. W. Pastor. 2005. Molecular dynamics simulations of the influenza hemagglutinin fusion peptide in micelles and bilayers: Conformational analysis of peptide and lipids. *J. Mol. Biol.* 354:1129–1141.

65. Zimmerberg, J., and M. M. Kozlov. 2006. How proteins produce cellular membrane curvature. *Nat. Rev. Mol. Cell Biol.* 7:9–19.

66. Haque, F., A. P. Pandey, …, J. S. Hovis. 2010. Adsorption of $\alpha$-synuclein on lipid bilayers: Modulating the structure and stability of protein assemblies. *J. Phys. Chem. B.* 114:4070–4081.

67. Reynolds, N. P., A. Soragni, …, S. Seeger. 2011. The mechanism of membrane interaction and disruption by $\alpha$-synuclein. *J. Am. Chem. Soc.* 133:19366–19375.

68. Tamm, L. K. 1994. Physical studies of peptide-bilayer interactions. *In* Membrane Protein Structure Experimental Approaches. S. H. White, editor. Oxford University Press, New York. 283–313.

69. Ben-Tal, N., B. Honig, …, S. McLaughlin. 1996. Binding of small basic peptides to membranes containing acidic lipids: Theoretical models and experimental results. *Biophys. J.* 71:561–575.

70. Perrin, R. J., W. S. Woods, …, J. M. George. 2000. Interaction of human $\alpha$-synuclein and Parkinson's disease variants with phospholipids. Structural analysis using site-directed mutagenesis. *J. Biol. Chem.* 275:34393–34398.

71. Callis, P. R., and T. Q. Liu. 2004. Quantitative prediction of fluorescence quantum yields for tryptophan in proteins. *J. Phys. Chem. B.* 108:4248–4259.

72. Takamori, S., M. Holt, …, R. Jahn. 2006. Molecular anatomy of a trafficking organelle. *Cell.* 127:831–846.

73. Ankner, J. F., and C. F. Majkrzak. 1992. Subsurface profile refinement for neutron specular reflectivity. *Proc. SPIE.* 1738:260–269.

74. Majkrzak, C. F., N. F. Berk, …, U. Perez-Salas. 2006. Structural investigation of membranes in biology by neutron reflectometry. *In* Neutron Scattering in Biology: Techniques and Applications. J. Fitter, T. Gutberlet, and J. Katsaras, editors. Springer, New York. 225–263.

75. Brooks, B. R., C. L. Brooks, 3rd, …, M. Karplus. 2009. CHARMM: the biomolecular simulation program. *J. Comput. Chem.* 30:1545–1614.

76. Jo, S., T. Kim, …, W. Im. 2008. Software news and updates—CHARMM-GUI: A web-based graphical user interface for CHARMM. *J. Comput. Chem.* 29:1859–1865.

77. MacKerell, A. D., D. Bashford, …, M. Karplus. 1998. All-atom empirical potential for molecular modeling and dynamics studies of proteins. *J. Phys. Chem. B.* 102:3586–3616.

78. Mackerell, Jr., A. D., M. Feig, and C. L. Brooks, 3rd. 2004. Extending the treatment of backbone energetics in protein force fields: Limitations of gas-phase quantum mechanics in reproducing protein conformational distributions in molecular dynamics simulations. *J. Comput. Chem.* 25:1400–1415.

79. Jorgensen, W. L., J. Chandrasekhar, …, M. L. Klein. 1983. Comparision of simple potential functions for simulating liquid water. *J. Chem. Phys.* 79:926–935.

80. Durell, S. R., B. R. Brooks, and A. Bennaim. 1994. Solvent-induced forces between 2 hydrophilic groups. *J. Phys. Chem.* 98:2198–2202.

81. Darden, T., D. York, and L. Pedersen. 1993. Particle mesh Ewald: An N.log(N) method for Ewald sums in large systems. *J. Chem. Phys.* 98:10089–10092.

82. Klauda, J. B., R. M. Venable, …, R. W. Pastor. 2010. Update of the CHARMM all-atom additive force field for lipids: Validation on six lipid types. *J. Phys. Chem. B.* 114:7830–7843.

83. Hoover, W. G. 1985. Canonical dynamics: Equilibrium phase-space distributions. *Phys. Rev. A.* 31:1695–1697.

84. Nose, S. 1984. A unified formulation of the constant temperature molecular-dynamics methods. *J. Chem. Phys.* 81:511–519.

85. Feller, S. E., Y. H. Zhang, …, B. R. Brooks. 1995. Constant pressure molecular dynamics simulation: The Langevin piston method. *J. Chem. Phys.* 103:4613–4621.

86. Ryckaert, J. P., G. Ciccotti, and H. J. C. Berendsen. 1977. Numerical integration of the Cartesian equations of motion of a system with constraints: Molecular dynamics of n-alkanes. *J. Comput. Phys.* 23:327–341.

87. Dolan, E. A., R. M. Venable, …, B. R. Brooks. 2002. Simulations of membranes and other interfacial systems using P2($_1$) and P*c* periodic boundary conditions. *Biophys. J.* 82:2317–2325.

88. Shirts, M. R., and J. D. Chodera. 2008. Statistically optimal analysis of samples from multiple equilibrium states. *J. Chem. Phys.* 129:124105.